Human Molecular Genetics, 2020, Vol. 29, No. 12 2065–2075

doi: 10.1093/hmg/ddaa094
Advance Access Publication Date: 18 May 2020
General Article

GENERAL ARTICLE

Colocalization of *Oxtr* with Prader-Willi syndrome transcripts in the trigeminal ganglion of neonatal mice

Radhika Vaidyanathan[1], Fabienne Schaller[2], Françoise Muscatelli[2] and Elizabeth A.D. Hammock[1,*,†]

[1]Department of Psychology and Program in Neuroscience, The Florida State University, Tallahassee, FL 32306, USA and [2]Aix-Marseille University UMR 1249, INSERM (Institut National de la Santé et de la Recherche Médicale) Unité 1249, INMED (Institut de Neurobiologie de la Méditerranée), Marseille, France

*To whom correspondence should be addressed at: 1107 West Call Street, Tallahassee, FL 32306, USA. Tel: +850 6459943; Fax: +850 6447739; Email: ehammock@fsu.edu

Abstract

Prader-Willi syndrome (PWS) is caused by deficient expression of the paternal copy of several contiguous genes on chromosome 15q11-q13 and affects multiple organ systems in the body, including the nervous system. Feeding and suckling deficits in infants with PWS are replaced with excessive feeding and obesity in childhood through adulthood. Clinical trials using intranasal oxytocin (OXT) show promise to improve feeding deficits in infants with PWS. The mechanism and location of action of exogenous OXT are unknown. We have recently shown in neonatal mice that OXT receptors (OXTR) are present in several regions of the face with direct roles in feeding. Here we show that the trigeminal ganglion, which provides sensory innervation to the face, is a rich source of *Oxtr* and a site of cellular co-expression with PWS gene transcripts. We also quantified OXTR ligand binding in mice deficient in *Magel2*, a PWS gene, within the trigeminal ganglion and regions that are anatomically relevant to feeding behavior and innervated by the trigeminal ganglion including the lateral periodontium, rostral periodontium, tongue, olfactory epithelium, whisker pads and brainstem. We found that peripheral OXTR ligand binding in the head is mostly intact in *Magel2*-deficient mice, although it is reduced in the lateral periodontium (gums) of neonatal *Magel2*-deficient mice compared to wild-type controls. These data suggest that OXT via orofacial OXTR may play a peripheral role to modulate sensory-motor reflexes necessary for suckling and may be part of the mechanism by which intranasal OXT shows promise for therapeutic benefit in PWS.

Introduction

Prader-Willi syndrome (PWS) is a multisystem disorder that affects 1 in 10 000–30 000 newborns (1). It is characterized by severe hypotonia of prenatal origin, poor oromotor suck leading to feeding deficiencies and poor weight gain in infancy (1). Many infants with PWS require assisted feeding using tubes to provide adequate food intake (2–5). However, the feeding deficit transforms into excessive feeding and obesity due to impaired satiety signals starting in childhood and progressing through adulthood. Hypothalamic dysfunction and impairment of the central oxytocin (OXT) system underlie many symptoms of PWS. For example, in postmortem studies, decreased OXT in the

†Elizabeth A.D. Hammock, http://orcid.org/0000-0001-7668-745X
Received: March 2, 2020. **Revised:** April 25, 2020. **Accepted:** May 12, 2020

paraventricular hypothalamic nucleus (PVN) (6,7) and reduced *Oxtr* gene expression in the frontal cortex (8) have been identified in separate cohorts of PWS patients.

PWS results from the lack of paternally inherited genes located on chromosome 15q11-q13 also known as the PWS-critical region (1,8). In a typical individual, 15q11-q13 is subject to genomic imprinting where the maternal copy is silenced and the paternal copy is active. The PWS-critical region contains the protein-coding genes, *MKRN3*, *MAGEL2*, *NDN*, *NPAP1* and *SNURF–SNRPN*, and a cluster of five repetitive snoRNA genes and several antisense transcripts (1,9). *MAGEL2* is selectively mutated (point mutations) in the closely related Schaaf-Yang syndrome which has a narrower phenotype but includes neonatal hypotonia and impaired feeding (9). Several mouse models have been created with targeted deletions of specific genes, and their phenotypes recapitulate many PWS symptoms (10; reviewed in 11, 12). Of these models, *Magel2*-deficient (Magel2P^{-}/M^{+}) mice (13) are a valuable model to investigate deficits in suckling behavior. The *Magel2* gene encodes a protein, belonging to the MAGE (melanoma antigen gene expression) gene family, that is important for endosomal trafficking (14). *Magel2*-deficient pups have very high postnatal lethality (50%) because of absent or weak suckling behavior. *Magel2*-deficient mice exhibit deficiencies in hypothalamic mature OXT with an accumulation of the immature OXT peptide, suggesting impaired posttranslational processing of OXT in the PVN (13,15). Interestingly, the suckling deficits and lethal feeding observed in *Magel2*-deficient pups are rescued by a single subcutaneous injection of OXT (2 µg in 20 µL 0.9% NaCl) 3–5 h after birth. Conversely, subcutaneous OXT receptor (OXTR) antagonist injections (3 µg in 20 µL 0.9% NaCl), within 1–1.5 h after birth to wild-type (WT) mice, prevent feeding and induce postnatal lethality (13). Intranasal delivery of OXT has been shown to be a promising therapeutic candidate for the treatment of feeding deficits in human clinical trials for infants with PWS (16), although further studies are needed with careful attention to participant age, OXT dose and therapeutic endpoints (17). The OXT system is well appreciated as a mediator of infant–parent bonding (18–24), and more recent evidence suggests that it also plays a role in sensory processing (25–28). If OXT rescues suckling behavior, then it suggests that OXT via OXTR modulates feeding circuits. The available evidence does not indicate where OXT will achieve this effect in the infant.

In neonatal mice, OXTR are expressed in the brain but also strongly expressed in several feeding-relevant peripheral regions in the face (29,30). Suckling is a bidirectional process that involves sensory cues from the mother that are detected by the infant to elicit a response (31). Specifically, the trigeminal nerve, hypoglossal nerve and facial nerve are involved in suckling behavior, as mutant mice with defects or injuries in these nerves exhibit suckling deficits (reviewed in (32)). *Oxtr* are expressed in the trigeminal ganglia (TG) in adult rodents (33) and pre-weaning mice, where orally applied OXT impacts brain activity (34), suggesting that OXTR on sensory neurons in the periphery might play an important role in the rescue of suckling defects by peripherally administered OXT.

To begin to address the possibility that the OXT system interacts with PWS transcripts in the periphery, we first determined if *Oxtr* colocalizes with PWS-critical gene transcripts in the TG because this is an anatomical region important for suckling and rooting behavior. Further, we determined if *Magel2* gene loss from the paternal locus influenced the abundance of OXTR in the periphery of neonatal mice, with emphasis on circuits involved in feeding and suckling behavior, using receptor autoradiography for OXTR in *Magel2*-deficient neonatal mice (13).

Results

Anatomy of oxytocin receptor mRNA and protein in the whole head at P0

At P0, we detect the presence of EGFP in the TG using Oxtr–EGFP reporter mice. EGFP-positive mice (Fig. 1A) but not EGFP-negative mice (Fig. 1B) show EGFP immunoreactivity in the TG and fiber projections to the face. At P0, we detect intense OXTR ligand binding (Fig. 1C and E) which is competed away by 1000 nM unlabeled OXT (Fig. 1D and F) in peripheral facial regions involved in feeding behavior. Despite the high levels of cytoplasmic EGFP reporter expression in the cell bodies of the TG, OXTR ligand binding is not robust in the TG (Figs 1C and 3E) but is instead present in innervation sites of the TG (orofacial targets and brainstem).

Anatomy of oxytocin receptor and Magel2 mRNA in the TG at P0

We performed chromogenic *in situ* hybridization (RNAscope) on the whole head of P0 mice for *Oxtr* and *Magel2* transcripts. We identified neurons in the TG of C57BL/6J WT male (Fig. 2A) and WT female (Fig. 2B) mice and FVB/N × Swiss Webster mice (Supplementary Material, Fig. S1) where *Oxtr* (red) and *Magel2* (blue-green) are co-expressed. We also validated the *Magel2*-deficient model by showing that they express *Oxtr* but not *Magel2* transcripts in the TG (Fig. 2C) and throughout the head.

Quantification of OXTR ligand binding in feeding-relevant peripheral regions in WT and Magel2-deficient neonates

To determine if loss of *Magel2* may influence the expression of OXTR in trigeminal target sites, we performed receptor autoradiography on *Magel2*-deficient and WT mice at P0 and quantified peripheral OXTR ligand binding in regions of the face relevant for feeding behavior. A significant decrease in OXTR ligand binding is observed in the lateral periodontium of *Magel2*-deficient mice compared to WT mice (two-tailed unpaired t-test, $^{*}P = 0.0314$, $t = 2.326$, $df = 17$, Cohen's $d = 1.057$) (Fig. 3A). OXTR ligand binding densities in the rostral periodontium (Fig. 3B), olfactory epithelium (Fig. 3C), tongue (Fig. 3D), TG (Fig. 3E) and whisker pads (Fig. 3F) of *Magel2*-deficient mice did not differ significantly from WT mice (Table 1). Further, we quantified the ciliary bodies in the eye (Supplementary Material, Fig. S2) that are not directly relevant to oromotor feeding behavior but have shown specific OXTR ligand binding previously (29). We did not detect any statistically significant differences between WT and *Magel2*-deficient mice in the ciliary bodies of the eye (Table 1).

In the brainstem (Fig. 3G), in the region receiving afferent fibers from the TG, OXTR ligand binding densities between WT and *Magel2*-deficient mice were not different (Table 1).

Anatomy of oxytocin receptor and other protein-coding gene transcripts from the PWS-critical region in the TG at P0

To determine if other protein-coding genes, from the PWS-critical locus (*Snrpn*, *Mkrn3*, *Ndn*) and the adjacent paternally silenced Angelman's locus (*Ube3a*), colocalize with *Oxtr* in the TG, we performed chromogenic *in situ* hybridization (RNAscope). At P0, *Oxtr* (red) transcripts also colocalize with *Snrpn/Snurf*, *Mkrn3*, *Ndn* and *Ube3a* (blue-green) in the TG of C57BL/6J mice (Fig. 4) and FVB/N × Swiss Webster mice (Supplementary Material, Fig. S3) at P0. Neurons in the TG co-expressing *Oxtr* and PWS

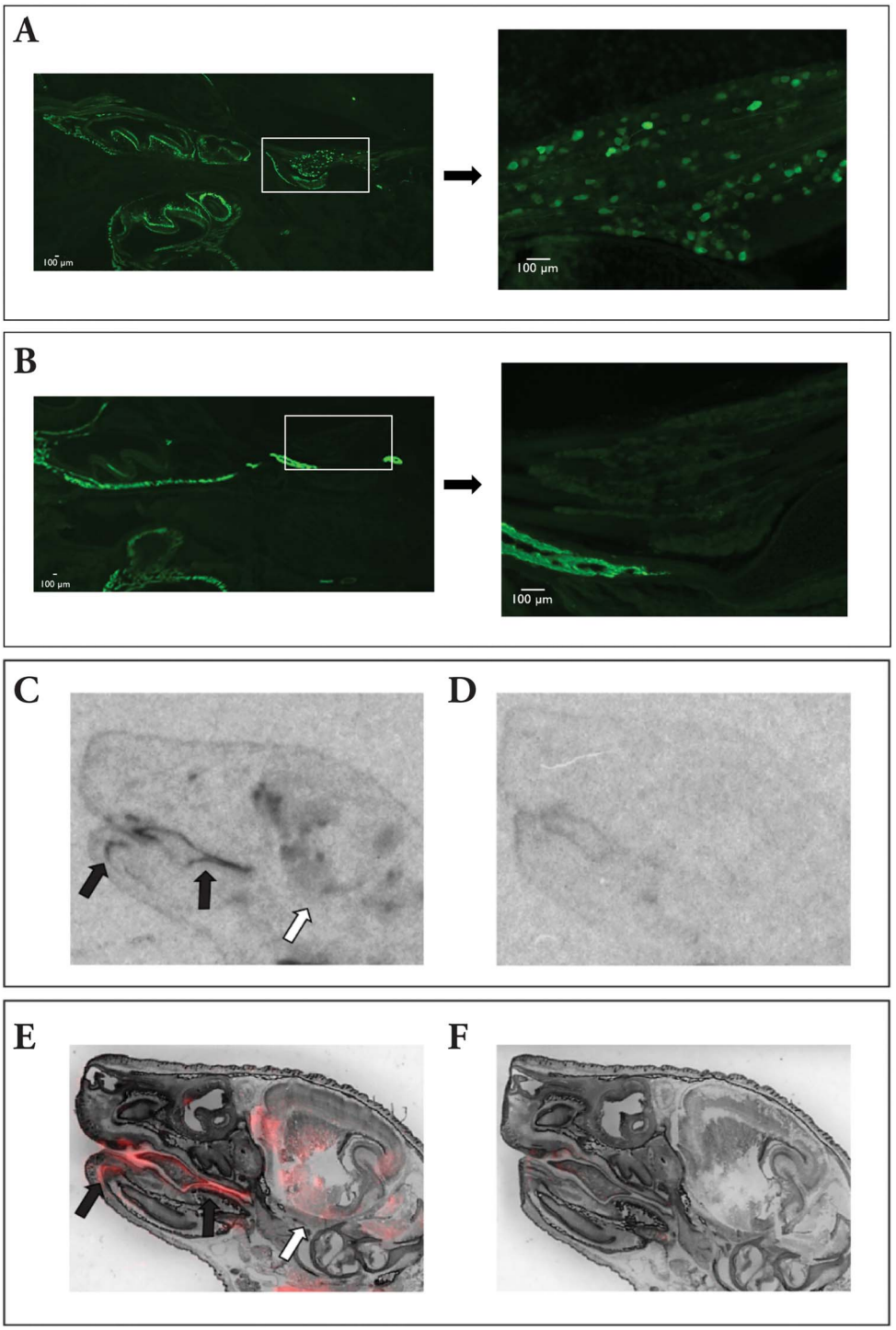

Figure 1. At postnatal day 0 (P0), the trigeminal ganglia express *Oxtr*, and peripheral targets of the trigeminal nerve display OXTR ligand binding. **(A)** *Oxtr*–EGFP reporter transgene-positive mice show EGFP immunoreactivity in the trigeminal ganglion (inset) with fiber projections to tissues of the face such as the primordial teeth and lateral periodontium, while transgene-negative mice **(B)** do not show EGFP immunoreactivity. **(C)** OXTR ligand binding in regions in the oral cavity (black arrows) and relative lack of OXTR binding in the trigeminal ganglion (white arrow). **(D)** Excess OXT (1000 nM) competes with radioligand to reduce the signal. **(E)** Pseudo-color composite (OXTR in red, cresyl violet counterstain in gray) with black arrows indicating robust OXTR ligand binding in the periodontium and the white arrow indicating modest OXTR binding in the trigeminal ganglion. **(F)** Pseudo-color composite of adjacent section stained with cresyl violet and OXTR ligand binding competed away with excess OXT.

or Angelman's transcripts were imaged at 40× magnification (Fig. 4A) to highlight individual cell bodies with co-expression (Fig. 4B). To determine if co-expression is specific to *Oxtr*, we also performed *in situ* hybridization with the PWS and AS probes and *Avpr1a* probe. We identified *Avpr1a*-positive neurons in the TG that colocalize with PWS and AS gene transcripts in the FVB/N × Swiss Webster strain at P0 (Supplementary Material, Fig. S3). However, the density of *Avpr1a*-positive

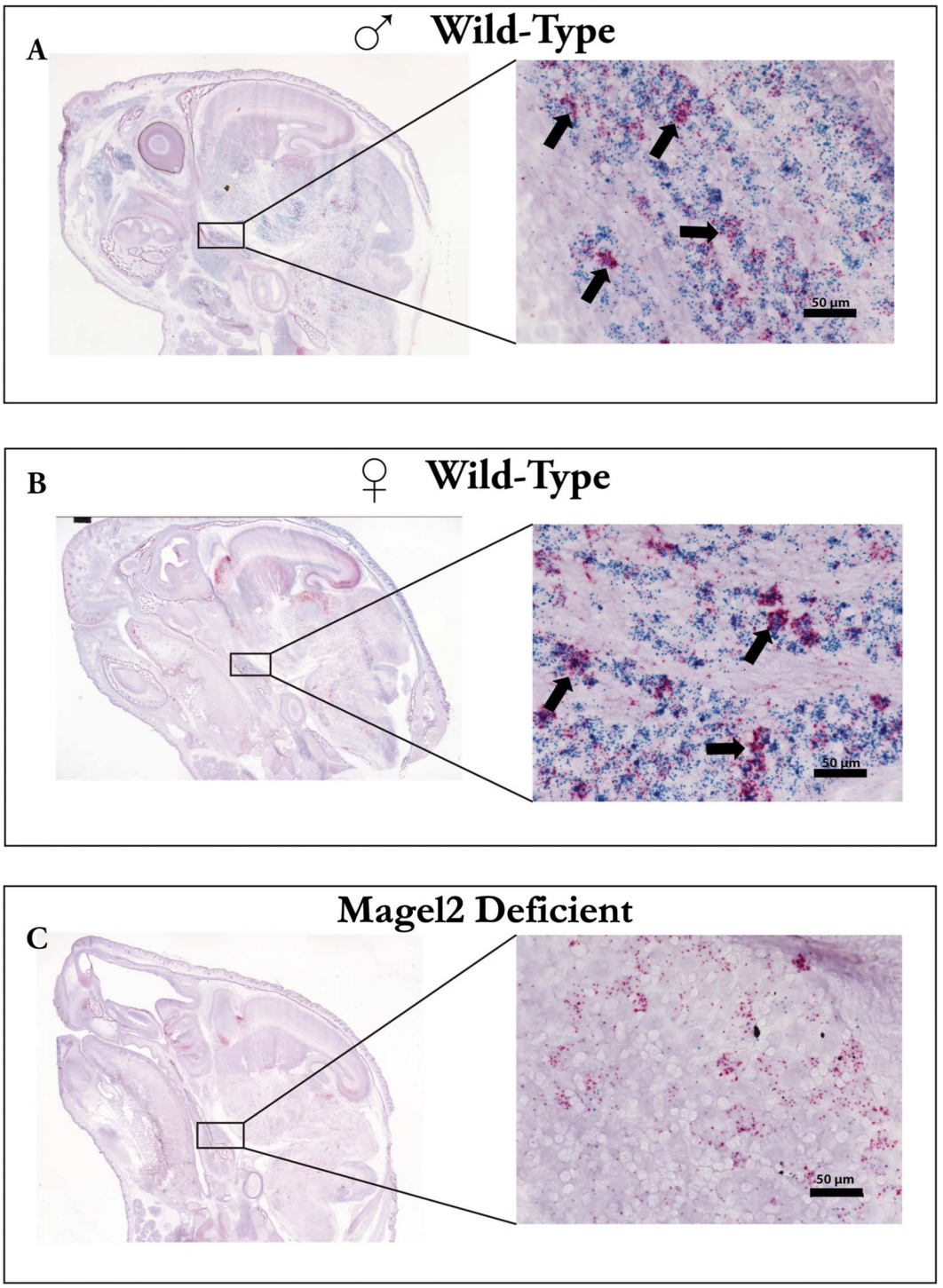

Figure 2. At postnatal day 0 (P0), *Oxtr* colocalizes with *Magel2* in the trigeminal ganglion of male and female WT mice. RNAscope *in situ* hybridization on sagittal sections reveals neurons in the trigeminal sensory ganglia co-express *Oxtr* (red) and *Magel2* (blue-green) transcripts in male (**A**) and female (**B**) C57BL/6J WT mice (examples indicated with black arrows). (**C**) Sagittal section of C57BL/6J *Magel2*-deficient male P0 mouse (left) and trigeminal ganglia (right) revealing neurons that express *Oxtr*, but do not express *Magel2*.

neurons was found to be much lower than *Oxtr*-positive neurons in the TG.

Anatomy of oxytocin receptor and Magel2 in the face at P0

To further investigate other regions in the periphery that express *Oxtr* and *Magel2*, we observed sagittal sections of whole head P0 in FVB/N × Swiss Webster mice following RNAscope *in situ* hybridization. The regions that were investigated for OXTR ligand binding also expressed *Oxtr* (red) and *Magel2* (blue-green) in proximity (Fig. 5). The tongue, the region dorsal to the lateral periodontium and the region rostral to the rostral periodontium have higher density of *Magel2* than *Oxtr*, while the olfactory epithelium, lateral periodontium and rostral periodontium have a higher density of *Oxtr* than *Magel2* (Fig. 5A–F).

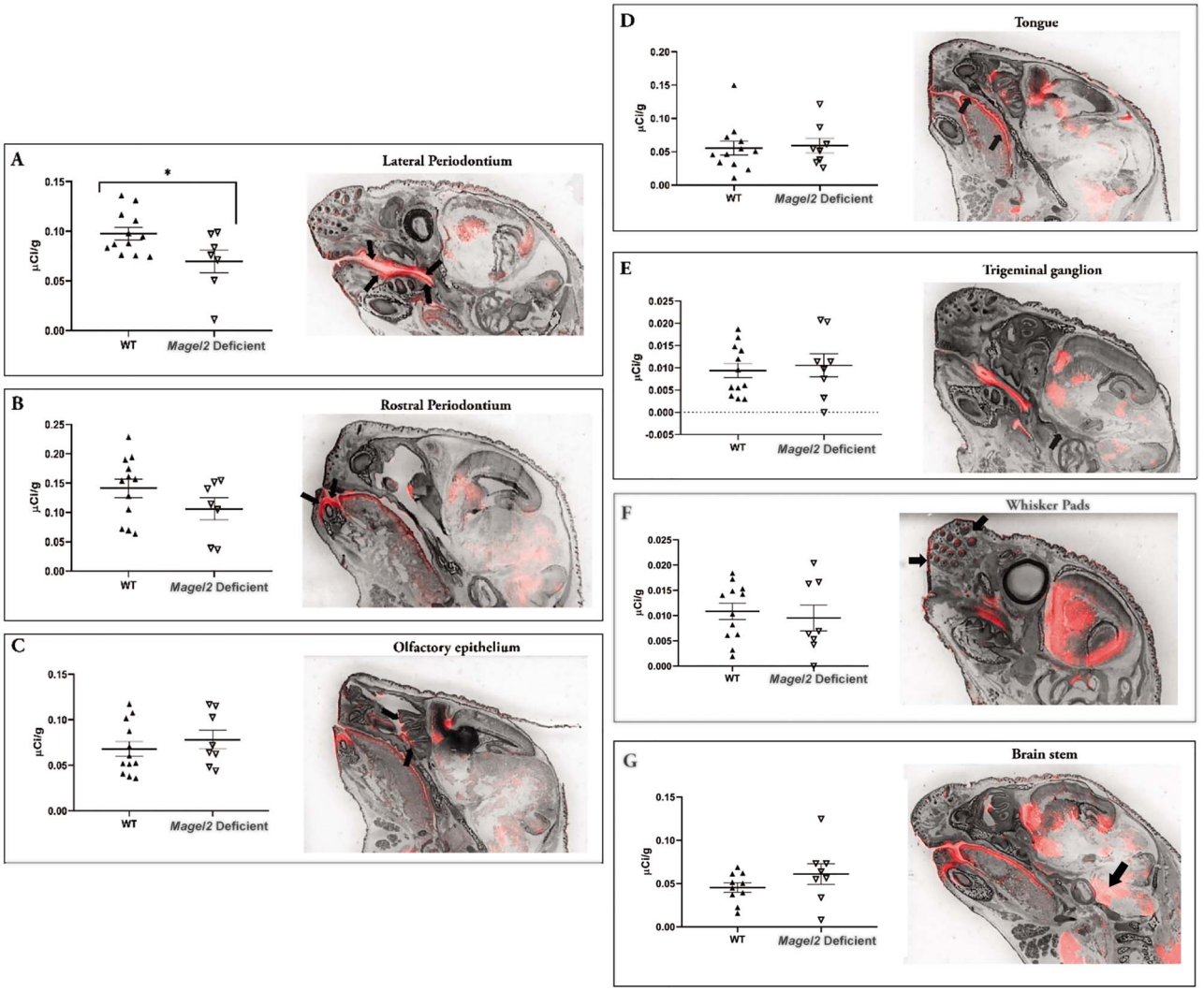

Figure 3. Loss of *Magel2* expression results in reduced OXTR ligand binding in the lateral periodontia, a feeding-related target of the trigeminal ganglia. Each panel presents a graph of quantified ligand binding on the left and a representative pseudo-colored composite image (OXTR in red, cresyl violet counterstain in gray) on the right with black arrows pointing to the quantified region. Specific OXTR binding values from each subject are plotted against the Y-axis. Group means, SEM and data points from independent subjects are plotted (WT (filled triangles), *Magel2*-deficient mice (open triangles)). (**A**) lateral periodontium, (**B**) rostral periodontium, (**C**) olfactory epithelium, (**D**) tongue, (**E**) trigeminal ganglion, (**F**) whisker pad and (**G**) brainstem. $^{*}P < 0.05$.

Table 1. Statistical analysis of ROI OXTR ligand-binding densities in WT versus Magel2 deficient mice

Region	*t* statistic	df	*P*-value	Cohen's *d*
Lateral periodontium	2.326	17	0.03*	1.057
Rostral periodontium	1.414	17	0.18	0.679
Olfactory epithelium	0.7751	18	0.78	0.353
Tongue	0.2449	18	0.81	0.113
Trigeminal ganglion	0.3234	17	0.75	0.146
Whisker pads	0.4548	18	0.45	0.113
Brainstem	1.283	16	0.22	0.585
Ciliary bodies	0.3752	17	0.71	0.181

$^{*}p$ value < 0.05.

Discussion

The current study highlights the potential relevance of peripheral circuits in PWS etiology. Oromotor circuits are the foundation of typical feeding behaviors, including suckling in infancy. Further, trigeminal activity influences the development of OXT production in the mouse hypothalamus in the first two postnatal weeks (26). Colocalization of *Oxtr* mRNA with PWS transcripts may permit an opportunity for OXT to rescue activity of the sensory component of oromotor feeding circuits. The primary goal of the current study is to identify regions in the periphery

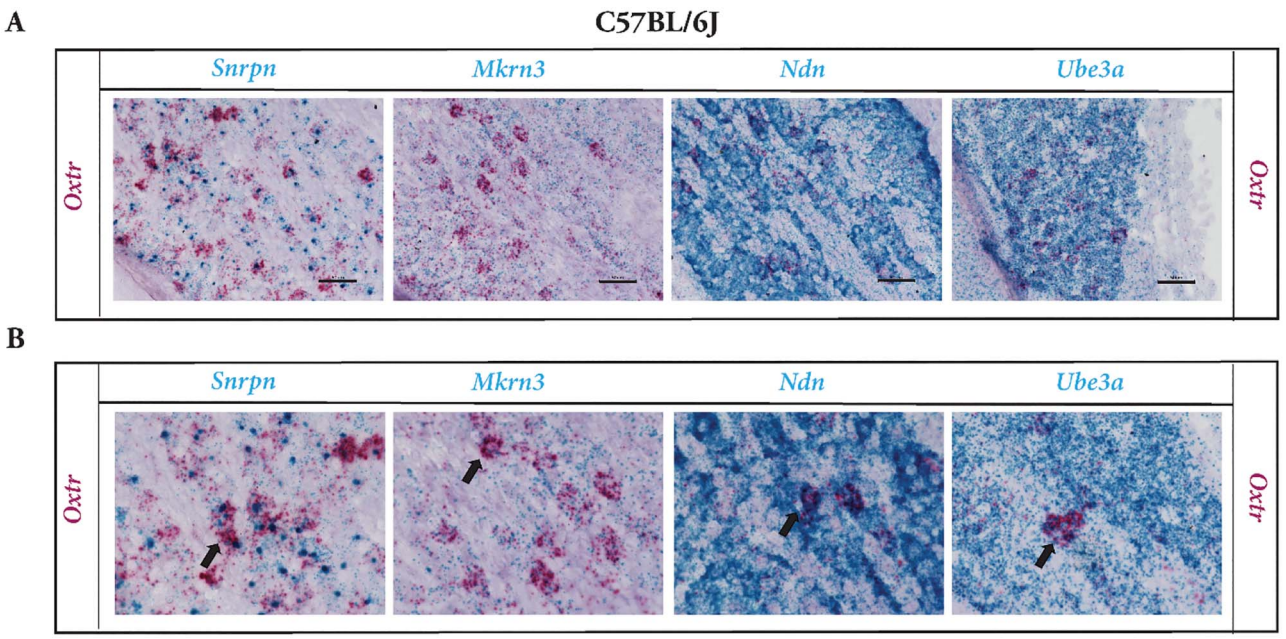

Figure 4. *Oxtr* colocalizes with *Snrpn/Snurf*, *Mkrn3*, *Ndn* and *Ube3a* in the trigeminal ganglion of C57BL/6J mice, suggesting a broader role for peripheral sensory ganglia in the developmental etiology of PWS. RNAscope *in situ* hybridization reveals neurons in the trigeminal sensory ganglia of a P0 mouse that co-express *Oxtr* and PWS gene transcripts, as well as *Ube3a* from the adjacent paternally silenced Angelman's syndrome locus. (**A**) Panel of sagittal sections (20 μm thickness) through the trigeminal ganglion indicates colocalization of *Oxtr* with four PWS gene transcripts in C57BL/6J P0 mouse. (**B**) Magnified view of neuronal cell bodies (black arrows) in the trigeminal ganglion revealing colocalization of *Oxtr* with *Snrpn/Snurf*, *Mkrn3*, *Ndn* and *Ube3a* in C57BL/6J P0 mouse. Scale bar 50 μm.

that may serve as targets for the therapeutic effects of exogenous OXT to alter signaling and/or activity in individuals deficient in the expression of PWS gene transcripts. We use a model system (*Magel2*-deficient mice) that has previously shown promise as a tool to understand the development of suckling behavior (13) and the role of OXT in the initiation of suckling. Although we have not addressed the mechanism of rescue of postnatal lethality in *Magel2*-deficient pups by OXT, we have initiated a series of necessary experiments to determine the relevance of peripheral OXTR in feeding-related circuit problems in infants with PWS. The findings of this study derive from three sets of experiments designed to determine: (A) if the *Oxtr* gene is expressed in the TG at P0 and if OXTR can be detected in the TG or the peripheral targets of TG, (B) if *Oxtr* is co-expressed with *Magel2* and other PWS gene transcripts in trigeminal sensory neurons involved in feeding behavior and (C) if endogenous OXTR ligand binding is altered in the feeding-relevant regions in the face of *Magel2*-deficient mice.

We identify the TG as a potentially important source of synthesis of *Oxtr* in P0 mice and emphasize that OXTR ligand binding is not present in equivalent abundance in the cell bodies of the TG itself. However, OXTR ligand binding is observed in several peripheral targets of the TG. While autoradiography lacks cellular level detail and we cannot determine the types of cells that express OXTR using this technique, we also cannot rule out the possibility that OXTR are expressed in the sensory nerve endings of TG neurons. Based on our anatomical observations, we hypothesize that *Oxtr* transcribed in the TG may be trafficked to TG nerve terminals where local translation may occur on demand or, alternatively, translated protein may be trafficked continuously to peripheral targets.

Strikingly, we identified intense expression of all the PWS gene transcripts including *Magel2*, as well as the maternally expressed Angelman's syndrome locus gene, *Ube3a*, in the TG at P0. Specifically, several neurons co-express *Oxtr* and the tested gene transcripts. These findings have important implications in the context of therapeutic effects of OXT via peripheral OXTR pathways in PWS and AS. Noticeably, we observed strain differences in the density of *Oxtr* in the TG with FVB/N × Swiss Webster pups having higher expression levels than C57BL/6J pups at P0 (Supplementary Material, Fig. S3). Because of the cross-sensitivity of OXT and vasopressin systems, we also tested colocalization of PWS gene transcripts with vasopressin 1A receptor transcripts (*Avpr1a*) and found that there are far fewer *Avpr1a*-positive neurons in the TG compared to *Oxtr*. However, some of these *Avpr1a* + neurons also express the tested PWS gene transcripts (Supplementary Material, Fig. S4).

To begin to test our hypothesis that *Oxtr* and *Magel2* colocalization in the trigeminal ganglion may be important for the mechanism of action of intranasal OXT in therapeutic effects in PWS, we measured peripheral OXTR ligand binding in WT and *Magel2*-deficient pups at P0. Because MAGEL2 may be involved in trafficking, one possible outcome would be massive reduction in OXTR ligand binding in the periphery of *Magel2*-deficient mice. However, if peripheral treatment with OXT rescues the lethal feeding effects of *Magel2*-deficient mice, the peripheral OXTR system would need to be roughly intact if this were the mechanism of action. Our OXTR autoradiography suggests a modest impairment in OXTR ligand binding, with only the lateral periodontium demonstrating a significant reduction in OXTR ligand binding. Although receptor autoradiography lacks the spatial resolution to identify specific cells in the anatomically broad periodontium, given that the periodontium is very heavily innervated by the TG, our data suggest that decreased OXTR ligand binding in the lateral periodontium of *Magel2*-deficient pups may be due to the loss of *Magel2* in the TG. We do not know how MAGEL2 might achieve an effect of decreased OXTR at the cell surface of the lateral periodontium. MAGEL2 may have a direct

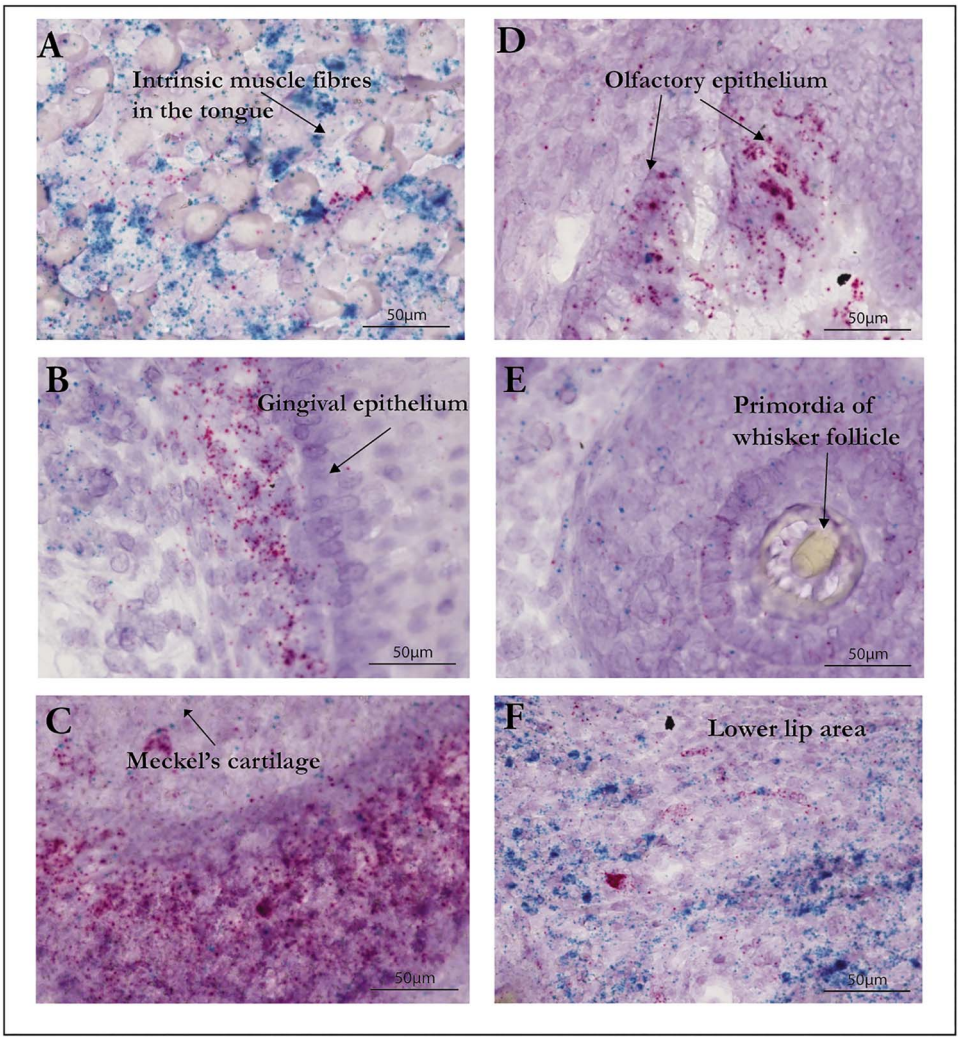

Figure 5. *Oxtr* and *Magel2* transcripts are expressed in peripheral tissues in close proximity in the neonatal mouse at P0. RNAscope *in situ* hybridization reveals *Oxtr* (red) and *Magel2* (blue-green) in cells of several peripheral tissues in the whole head of a P0 FVB/N × Swiss Webster WT male mouse. Scale bar 50 μm. **(A)** Tongue cells widely express *Magel2* and relatively fewer *Oxtr* transcripts. **(B)** Lateral periodontium expresses higher levels of *Oxtr*, and *Magel2* transcripts are detected dorsal to the periodontium (located to the left on the figure). **(C)** Rostral periodontium predominantly expresses *Oxtr* and few *Magel2* transcripts. **(D)** Olfactory epithelium cells express higher levels of *Oxtr* than *Magel2*. **(E)** Whisker pad expresses few *Oxtr* and *Magel2*. **(F)** Area adjacent (rostral) to rostral periodontium expresses *Magel2* and *Oxtr*.

effect of *Oxtr* gene expression or alter OXTR presentation on the cell surface without modifying *Oxtr* gene expression. MAGEL2 regulates receptor internalization, intracellular trafficking and degradation to modify the leptin receptor availability at the cell surface (35). Mutations in *Magel2* prevent the MAGEL2-mediated increase of leptin receptors on the cell surface of hypothalamic neurons (35). Perhaps MAGEL2 function in the TG is required to regulate receptor trafficking through the intricate fiber network innervating the periodontium. It is also possible that rather than affecting *Oxtr* mRNA or OXTR protein trafficking from the TG, MAGEL2 is involved in regulating OXTR in local (non-neural) tissues of the mouth. Of note, the OXTR ligand binding capacity of the orofacial regions, as a whole, remained relatively intact, indicating the possibility of a peripheral mechanism of rescue by OXT in the *Magel2*-deficient mouse.

Our study, while permissive, does not necessarily imply a causal link between the reduced OXTR levels in the lateral periodontia and suckling deficits in *Magel2*-deficient pups. Instead, our main finding is that PWS transcripts are enriched in sensory neurons of an oromotor circuit for suckling, including OXTR-expressing cells, indicating that these cells may be a target for OXT therapy. This suggests that in future experiments, we should investigate if a selective deletion of *Magel2* in peripheral sensory ganglia, including the trigeminal ganglia, is sufficient to impair feeding, social behavior and hypothalamic development as seen in PWS. In mouse models of autism spectrum disorders, a similar observation has been made regarding restricted impairment in peripheral sensory ganglia contributing to behavior and brain dysfunction (36) which aligns with a developmental diaschisis model of neurodevelopmental disorders (37).

Limitations of this study include the lack of cellular resolution of receptor autoradiography which could be remedied by the use of specific anti-OXTR antibodies for protein colocalization studies and that our sample size for *Magel2*-deficient pups was derived from a population with mixed phenotypes (with and without suckling deficits) due to sample collection at P0. We may observe a different result if our sample size was derived entirely from the population of *Magel2* deficient with suckling deficits. In the *Magel2*-deficient mouse line used in our study, only 50% are

expected to survive beyond P1. Because we cannot yet predict a priori which mice will not survive, the *Magel2*-deficient mice in this study are a mix of mice that have moderate to lethal impairments in suckling. This may have reduced the observed effect size of *Magel2* deletion on OXTR ligand binding in the periodontium for neonates at risk or potentially masked *Magel2*-deficient effects in other important areas. There were no areas where *Magel2*-deficient mice showed significantly more ligand binding. Further, we quantified OXTR ligand binding in other TG facial targets that are less directly involved in feeding behavior such as the ciliary bodies of the eye and did not observe a significant reduction in the *Magel2*-deficient pups (Supplementary Material, Figure S2A and B). MAGEL2 may play roles other than mRNA or protein trafficking and may be involved in the cell signaling after OXTR activation. Despite these limitations, this study confirms that *Oxtr* and PWS transcripts colocalize to sensory neurons of the trigeminal ganglion innervating the face and suggests that PWS phenotypes and potential therapeutic effects of OXT may begin in the periphery.

To conclude, in this study we identify the TG as an anatomical site in the peripheral nervous system where OXT via OXTR may regulate feeding circuits potentially involving cross talk with MAGEL2 and other PWS gene products. These feeding circuits may enhance the experience-dependent development of OXT in the hypothalamus (26), which is altered in PWS (6), in *Magel2*-deficient mice (13) and *Oxtr* KO mice (38). In addition to colocalization of *Oxtr* and *Avpr1a* transcripts with PWS transcripts in the TG, we observed a decrease in OXTR ligand binding in *Magel2*-deficient neonates in the lateral periodontium, which is densely innervated by the mandibular and maxillary branches of the TG. We theorize that exogenous OXT helps to stimulate peripheral sensory neurons via OXTR to compensate for what may be atypical function in *Magel2*-deficient pups. The presence of *Avpr1a* mRNA in these circuits also suggests a potential explanation for blunted or adverse effects in OXT therapeutics if stimulation of this receptor opposes the actions of OXTR. A recent double-blind placebo-controlled clinical trial with intranasal carbetocin, a selective OXTR agonist (39), indicates therapeutic benefit in 10- to 18-year-old individuals with PWS (40). These observations suggest that peripheral pathways should be given consideration in attempts to understand PWS phenotypes and OXT-based therapies. Indeed, prior evidence indicates that the PWS gene *Necdin* regulates peripheral sensory neuron development in mice (41). Sensory deprivation in the neonatal period has been shown to impair hypothalamic OXT production in mice (26). From this viewpoint, PWS may represent a genetic form of perinatal sensory deprivation.

Materials and Methods

Mice

All procedures in live mice at Florida State University were performed after approval by the Institutional Animal Care and Use Committee, Florida State University (protocol #1722 and #1746), in accordance with state and federal guidelines (Guide for the Care and Use of Laboratory Animals of the National Institutes of Health). The GENSAT consortium created the Oxtr–EGFP mouse from a BAC clone containing EGFP downstream of the *Oxtr* regulatory region, with construct injection into FVB/N pronuclei and maintenance on a mixed FVB/N × Swiss Webster background (42). These mice were bred within our laboratory by mating hemizygous EGFP males with wild-type (WT) females from this line. WT littermates were used as controls for EGFP antibody staining and endogenous expression. *Magel2*-deficient mice were bred from mice generated as described previously (13), and WT and mutant mice were bred in INMED animal facility (Marseille) after backcrossing to C57BL/6J. Mice were handled and cared for in accordance with the Guide for the Care and Use of Laboratory Animals (N.R.C., 1996) and the European Communities Council Directive of September 22, 2010 (2010/63/EU, 74). Experimental protocols were approved by the institutional ethics committee guidelines for animal research with the APAFIS accreditation no. 13455 from the French Ministry of Agriculture. We maintain group-housed mice (3–5 mice/cage). All efforts were made to minimize the number of animals used. *Magel2* mutant heterozygous mice were maintained on a C57BL/6J background by crossing heterozygous *Magel2* mutant females (*Magel2*$^{m-/p+}$) with WT males. Since *Magel2* undergoes genomic imprinting, with expression of the inherited paternal allele only, heterozygous mice carrying a maternally transmitted mutant *Magel2* allele (*Magel2*$^{m-/p+}$) are functionally equivalent to WT mice. Male progeny carrying the maternal mutant allele (*Magel2*$^{m-/p+}$) were crossed with WT C57BL/6J females to generate WT and heterozygous (*Magel2*$^{m+/p-}$) littermates with paternal transmission of the mutant allele. Frozen neonatal specimens were shipped to Florida State University.

Genotype and sex determination

Genomic DNA was collected from tail samples for genotyping for sex and Oxtr–EGFP by PCR (30). Briefly, to determine genetic sex of neonates, the forward primer (5′-ccgctgccaaattctttgg-3′) and the reverse primer (5′-tgaagcttttggctttgag-3′) generated a 290 bp product from the *Smcy* gene on the Y chromosome and a 330 bp product from the *Smcx* homolog on the X chromosome under the following thermal cycling conditions: 95°C for 7 min; 35 cycles of 93°C for 30 s, 58°C for 30 s and 72°C for 30 s; and 72°C for 10 min. To determine the genotype of Oxtr–EGFP mice, we used the forward primer (5′-gccacactttaaagagcctcaa-3′) and reverse primer (5′-tagcggctgaagcactgca-3′) to generate a 320 bp transgene band under the following thermal cycling conditions: initial hot start at 94°C for 5 min and 10 cycles of touch down PCR at 94°C for 15 s, 65°C–1°/cycle for 30 s and 72°C for 40 s, followed by 30 cycles of 94°C for 15 s, 55°C for 30 s, 72°C for 40 s and 72°C for 5 min. The *Magel2* locus was genotyped by PCR, using the forward primer (5′-ccctgggttgactgactcat-3′) and reverse primer (5′-tcttcttccttggtggctttg-3′) to generate a 376 bp PCR product, as described previously (13).

EGFP immunohistochemistry

To amplify the endogenous EGFP signal for fluorescence microscopy, whole heads were used in immunohistochemistry. Neonates were transcardially perfused with 0.1 M phosphate buffer pH 7.4, followed by 4% PFA, pH 7.4 at P0. Fixed and cryoprotected tissue was cryosectioned at 20 µm in six series in the sagittal plane onto the SuperFrost Plus slides. Slides were washed in PBS with 0.25% Triton X-100 4 × 15 min and then incubated in sodium borohydride (0.5 g/100 mL PBS) for 20 min. Detergent was eliminated from all subsequent steps. Slides were washed 4 × 15 min in PBS and blocked with 2% BSA in PBS prior to antibody incubation. Slides were incubated with 1:1000 chicken anti-GFP primary antibody (Abcam #ab13970) in 2% BSA overnight at 4°C in a humidified chamber. After incubation, slides were washed 5 × 5 min in PBS and incubated with 1:1000 Alexa 488 donkey anti-chicken secondary antibody (Affinity Pure) in 2% BSA in PBS for 1 h. Slides were washed 5 × 5 min in PBS, air-dried and coverslipped with Vectashield (Vector

Laboratories, CA, USA). Images were captured on a fluorescence microscope (Keyence BZ-X710, Keyence Corp., Osaka, Japan).

Chromogenic *in situ* hybridization

Fresh frozen tissue was cryosectioned in six series at 20 µm in the sagittal plane and mounted on SuperFrost Plus slides. Sections were stored at −80°C until used for RNA detection. RNA detection was performed on tissue sections using RNAscope 2.5HD Duplex Assay (Cat. No. 322430, Advanced Cell Diagnostics (ACD), Hayward, CA). The six probes used are synthetic oligonucleotide probes complementary to the nucleotide sequence 1198–2221 of *Oxtr* (NM_001081147.1; Oxtr-E4-C2, ACD Cat. No. 411101-C2), 3229–4220 of *Magel2* (NM_013779.2; Magel2-01, ACD Cat. No. 535901), 1501–2550 of *Mkrn3* (NM_011746.2; Mkrn3, ACD Cat no. 535911), 52–1324 of *Ndn* (NM_010882.3; NDN, ACD Cat no. 442711) and 1400–2020 of *Snrpn/Snurf* (NM_033174.3; SNRPN/SNURF, ACD Cat no. 535921), 1600–2850 of *Ube3a* (NM_173010.3; Ube3a, ACD Cat. No. 536021) and 821–2017 of *Avpr1a* (NM_016847.2; Avpr1a, ACD Cat. No. 418061-C2). Briefly, slides were fixed in 4% paraformaldehyde in PBS (pH 9.5) on ice for 2 h and dehydrated in increasing concentrations of alcohol and then stored in 100% ethanol overnight at −20°C. The slides were air-dried for 10 min and then pretreated in target retrieval solution (Ref. 322 001, ACD) for 5 min while boiling, after which, slides were rinsed two times in water and then 100% ethanol and air-dried. A hydrophobic barrier pen (ImmEdge) was used to create a barrier around selected sections. Selected sections were then incubated with Protease Plus (Ref. 322 331, ACD) for 15 min in a HybEZ oven (ACD) at 40°C, followed by water washes. The sections were then hybridized with the probe mixture at 40°C for 2 h per slide. Unbound hybridization probes were removed by washing two times in wash buffer and incubated overnight in 5× SSC. After hybridization, sections were subjected to signal amplification using the HD 2.5 detection kit following the kit protocol. Hybridization signal was detected using a mixture of Fast-RED solutions A and B (60:1) for *Oxtr* or *Avpr1a* and a mixture of Green Solutions A and B (50:1) for *Magel2*, *Mkrn3*, *Snrpn/Snurf*, *Ndn* or *Ube3*a such that each section had only one combination of red and blue-green probe signal. The slides were then counterstained with Gill's hematoxylin (American Mastertech Scientific, Inc. Lodi, CA) and air-dried in a 60°C oven for 15 min. Slides were cooled and coverslipped with Vectamount™ (Vector Laboratories, Inc. Burlingame, CA). Slides were imaged at 4× and 10× on a bright-field microscope (Keyence BZ-X710, Keyence Corp., Osaka, Japan). P0 whole head sagittal sections were investigated for colocalization of *Oxtr* or *Avpr1a* (red) with each PWS/*Ube3a* (blue-green) transcript.

Receptor autoradiography

Fresh frozen tissue was cryosectioned in six series at 20 µm in the sagittal plane and mounted on SuperFrost Plus slides. Sections were stored at −80°C until used in the receptor autoradiography protocol. Receptor autoradiography used 0.05 nM ^{125}I labeled OXT receptor ligand (iodinated–ornithine vasotocin analog [^{125}I]-OVTA (43,44); NEX254, PerkinElmer, Waltham, MA) performed by standard methods (30). Non-specific tissue binding in the periphery of the neonatal mouse was assessed by adding 1000 nM of unlabeled OXT peptide (oxytocin acetate salt hydrate, Cat. No. O6379, Sigma-Aldrich, St. Louis, MO). Unlabeled OXT peptide competed away the [^{125}I]-OVTA in regions of high binding specificity. Regions that were not competed away by unlabeled OXT were identified as regions of non-specific binding. The competition dose was determined by previous experiments with WT and OXTR knockout mice (29). Autoradiographic films (Kodak BioMax MR film, Carestream Health, Inc., Rochester, NY, USA) were exposed to slides and ^{14}C autoradiographic standards (ARC-0146; American Radiolabeled Chemicals, St. Louis, MO, USA) for 10 days before development (Mini-Medical/90 X-ray film processor, AFP Imaging, New York).

Image analysis

Following autoradiography, all slides were stained with cresyl violet for accurate and unbiased region of interest measurements. Briefly, slides were incubated in 0.5% cresyl violet solution at 37°C for 5 min, rinsed in deionized water, differentiated in 95% ethanol in two 5 min washes and dehydrated in 100% ethanol in two 5 min washes. Slides were then cleared in CitriSolv (Decon Labs Inc., King of Prussia, PA) in two 5 min washes and coverslipped. Developed films and stained slides were scanned on a flatbed scanner at 1200 dpi (Epson, Epson Perfection V600 Photo). Regions of interest were identified on cresyl violet-stained slides, and measurements were collected from corresponding film images. Region of interest quantifications were recorded in ImageJ (NIH, Bethesda, MD) using the brush selection tool, from three consecutive sections within each animal. Local background values were obtained from a non-tissue background of the film adjacent to the region of interest and measured in a 20×20 pixel region and then subtracted from the region of interest values to generate local densitometry values. Ligand binding values in µCi/gram were calculated by interpolation 'interp1,' MatLab 8.1.0 (TheMathWorks, Natick, MA, USA) to the linear range of the ^{14}C autoradiographic standard on the same film (45). Specific ligand binding values (µCi/gram) were generated by subtracting ligand binding values (µCi/gram) of films with competition binding from ligand binding values (µCi/gram) of corresponding films with labeled OXTR signal. For quantification, no image adjustments were made except image inversion so that higher numbers represented more dense binding. Composite images were created using the TurboReg (46) plug-in for ImageJ using the rigid-body alignment algorithm. For pseudo-color composites, the autoradiography images were adjusted for brightness to minimize the appearance of the film background.

Statistical analysis

Values for specific OXTR ligand binding from individual regions of interest were tested for normality and analyzed by two-tailed unpaired t-tests using GraphPad Prism 8.1.1. We analyzed WT ($n = 12$) pups and *Magel2*-deficient ($n = 8$) pups, and we were underpowered to detect modest sex differences and therefore did not include sex as an independent variable in our statistical analysis. Some tissue sections were damaged and could not be quantified. This reduced the effective sample size to seven *Magel2*-deficient mice for two regions.

Supplementary Material

Supplementary Material is available at *HMG* online.

Acknowledgements

The authors would like to thank Esther A.R. Forti, Noelle Lewis and Chloe Johnson for their technical assistance and the animal care staff at Florida State University for animal husbandry.

Conflicts of Interest Statement. Fabienne Schaller and Françoise Muscatelli are co-inventors on a patent to use oxytocin in the

treatment of infant feeding disorder, e.g. Prader-Willi Syndrome (No. WO/2011/147889; US/2014/US9125862B2). The other authors have indicated they have no potential conflicts of interest to disclose.

Funding

Support for this work was provided by a grant from the Foundation for Prader-Willi Research (to E.A.D.H.) and Florida State University.

References

1. Cassidy, S.B., Schwartz, S., Miller, J.L. and Driscoll, D.J. (2012) Prader-Willi syndrome. *Genet. Med.*, **14**, 10–26.
2. Neo, W.S. and Tonnsen, B.L. (2019) Brief report: challenging behaviors in toddlers and preschoolers with Angelman, Prader-Willi, and Williams syndromes. *J. Autism Dev. Disord.*, **49**, 1717–1726.
3. Miller, J.L., Lynn, C.H., Driscoll, D.C., Goldstone, A.P., Gold, J.-A., Kimonis, V., Dykens, E., Butler, M.G., Shuster, J.J. and Driscoll, D.J. (2011) Nutritional phases in Prader-Willi syndrome. *Am. J. Med. Genet. A*, **155A**, 1040–1049.
4. Chu, C.E., Cooke, A., Stephenson, J.B., Tolmie, J.L., Clarke, B., Parry-Jones, W.L., Connor, J.M. and Donaldson, M.D. (1994) Diagnosis in Prader-Willi syndrome. *Arch. Dis. Child.*, **71**, 441–442.
5. Stevenson, D.A., Anaya, T.M., Clayton-Smith, J., Hall, B.D., Van Allen, M.I., Zori, R.T., Zackai, E.H., Frank, G. and Clericuzio, C.L. (2004) Unexpected death and critical illness in Prader–Willi syndrome: report of ten individuals. *Am. J. Med. Genet. A*, **124A**, 158–164.
6. Swaab, D.F., Purba, J.S. and Hofman, M.A. (1995) Alterations in the hypothalamic paraventricular nucleus and its oxytcoin neurons(putative satiety cells) in Prader-Willi syndrome: a study of five cases. *J. Clin. Endocrinol. Metabol.*, **80**, 573–579.
7. Swaab, D. (1997) Prader—Willi syndrome and the hypothalamus. *Acta Paediatr.*, **86**, 50–54.
8. Bittel, D.C. and Butler, M.G. (2005) Prader–Willi syndrome: clinical genetics, cytogenetics and molecular biology. *Expert Rev. Mol. Med.*, **7**, 1–20.
9. Fountain, M.D. and Schaaf, C.P. (2016) Prader-Willi syndrome and Schaaf-Yang syndrome: neurodevelopmental diseases intersecting at the MAGEL2 gene. *Diseases*, **4**, 2.
10. Chamberlain, S.J. and Brannan, C.I. (2001) The Prader-Willi syndrome imprinting center activates the paternally expressed murine Ube3a antisense transcript but represses paternal Ube3a. *Genomics*, **73**, 316–322.
11. Resnick, J., Nicholls, R. and Wevrick, R. Prader-Willi syndrome animal models working Group2013. Recommendations for the investigation of animal models of Prader-Willi syndrome. *Mamm. Genome*, **24**, 165–178.
12. Carias, K.V. and Wevrick, R. (2019) Preclinical testing in translational animal models of Prader-Willi syndrome: overview and gap analysis. *Mol. Ther. Methods Clin. Dev.*, **13**, 344–358.
13. Schaller, F., Watrin, F., Sturny, R., Massacrier, A., Szepetowski, P. and Muscatelli, F. (2010) A single postnatal injection of oxytocin rescues the lethal feeding behaviour in mouse newborns deficient for the imprinted Magel2 gene. *Hum. Mol. Genet.*, **19**, 4895–4905.
14. Hao, Y.H., Doyle, J.M., Ramanathan, S., Gomez, T.S., Jia, D., Xu, M., Chen, Z.J., Billadeau, D.D., Rosen, M.K. and Potts, P.R. (2013) Regulation of WASH-dependent actin polymerization and protein trafficking by ubiquitination. *Cell*, **152**, 1051–1064.
15. Grinevich, V., Knobloch-Bollmann, H.S., Eliava, M., Busnelli, M. and Chini, B. (2016) Assembling the puzzle: pathways of oxytocin signaling in the brain. *Biol. Psychiatry*, **79**, 155–164.
16. Tauber, M., Boulanouar, K., Diene, G., Çabal-Berthoumieu, S., Ehlinger, V., Fichaux-Bourin, P., Molinas, C., Faye, S., Valette, M., Pourrinet, J. *et al.* (2017) The use of oxytocin to improve feeding and social skills in infants with Prader–Willi syndrome. *Pediatrics*, **139**, e20162976.
17. Rice, L.J., Einfeld, S.L., Hu, N. and Carter, C.S. (2018) A review of clinical trials of oxytocin in Prader-Willi syndrome. *Curr Opin Psychiatry*, **31**, 123–127.
18. Alves, E., Fielder, A., Ghabriel, N., Sawyer, M. and Buisman-Pijlman, F.T. (2015) Early social environment affects the endogenous oxytocin system: a review and future directions. *Front. Endocrinol (Lausanne)*, **6**, 32.
19. Bales, K.L. and Carter, C.S. (2003) Sex differences and developmental effects of oxytocin on aggression and social behavior in prairie voles (Microtus ochrogaster). *Horm. Behav.*, **44**, 178–184.
20. Champagne, F., Diorio, J., Sharma, S. and Meaney, M.J. (2001) Naturally occurring variations in maternal behavior in the rat are associated with differences in estrogen-inducible central oxytocin receptors. *Proc. Natl. Acad. Sci. U. S. A.*, **98**, 12736–12741.
21. Carter, C.S. (2003) Developmental consequences of oxytocin. *Physiol. Behav.*, **79**, 383–397.
22. Vaidyanathan, R. and Hammock, E.A. (2017) Oxytocin receptor dynamics in the brain across development and species. *Dev. Neurobiol.*, **77**, 143–157.
23. Hammock, E.A. (2015) Developmental perspectives on oxytocin and vasopressin. *Neuropsychopharmacology*, **40**, 24–42.
24. Kojima, S., Stewart, R.A., Demas, G.E. and Alberts, J.R. (2012) Maternal contact differentially modulates central and peripheral oxytocin in rat pups during a brief regime of mother-pup interaction that induces a filial huddling preference. *J. Neuroendocrinol.*, **24**, 831–840.
25. Oettl, L.L., Ravi, N., Schneider, M., Scheller, M.F., Schneider, P., Mitre, M., da Silva Gouveia, M., Froemke, R.C., Chao, M.V., Young, W.S. *et al.* (2016) Oxytocin enhances social recognition by modulating cortical control of early olfactory processing. *Neuron*, **90**, 609–621.
26. Zheng, J.J., Li, S.J., Zhang, X.D., Miao, W.Y., Zhang, D., Yao, H. and Yu, X. (2014) Oxytocin mediates early experience-dependent cross-modal plasticity in the sensory cortices. *Nat. Neurosci.*, **17**, 391–399.
27. Bianca, J., Marlin, M.M., D'amour, J.A., Chao, M.V. and Froemke, R.C. (2015) Oxytocin enables maternal behavior by balancing cortical inhibition. *Nature*, **520**, 499–504.
28. Grinevich, V. and Stoop, R. (2018) Interplay between oxytocin and sensory systems in the orchestration of socio-emotional behaviors. *Neuron*, **99**, 887–904.
29. Greenwood, M.A. and Hammock, E.A. (2017) Oxytocin receptor binding sites in the periphery of the neonatal mouse. *PLoS One*, **12**, e0172904.
30. Hammock, E.A. and Levitt, P. (2013) Oxytocin receptor ligand binding in embryonic tissue and postnatal brain development of the C57BL/6J mouse. *Front. Behav. Neurosci.*, **7**, 195.
31. Syrina Al Ain, L.B., Schaal, B. and Patris, B. (2013) How does a newly born mouse get to he nipple? Odor substrates eliciting first nipple grasping and sucking responses. *Dev. Psychobiol.*, **55**, 888–901.

32. Muscatelli, F. and Bouret, S.G. (2018) Wired for eating: how is an active feeding circuitry established in the postnatal brain? *Curr. Opin. Neurobiol.*, **52**, 165–171.
33. Lopes, D.M., Denk, F. and McMahon, S.B. (2017) The molecular fingerprint of dorsal root and trigeminal ganglion neurons. *Front. Mol. Neurosci.*, **10**, 304–304.
34. Tabbaa, M. and Hammock, E.A. (2020) Orally administered oxytocin alters brain activation and behaviors of pre-weaning mice. *Horm. Behav.*, **118**, 104613.
35. Wijesuriya, T.M., De Ceuninck, L., Masschaele, D., Sanderson, M.R., Carias, K.V., Tavernier, J. and Wevrick, R. (2017) The Prader-Willi syndrome proteins MAGEL2 and necdin regulate leptin receptor cell surface abundance through ubiquitination pathways. *Hum. Mol. Genet.*, **26**, 4215–4230.
36. Orefice, L.L., Zimmerman, A.L., Chirila, A.M., Sleboda, S.J., Head, J.P. and Ginty, D.D. (2016) Peripheral mechanosensory neuron dysfunction underlies tactile and behavioral deficits in mouse models of ASDs. *Cell*, **166**, 299–313.
37. Wang, S.S.-H., Kloth, A.D. and Badura, A. (2014) The cerebellum, sensitive periods, and autism. *Neuron*, **83**, 518–532.
38. Vaidyanathan, R. and Hammock, E.A. (2020) Oxytocin receptor gene loss influences expression of the oxytocin gene in C57BL/6j mice in a sex-and age-dependent manner. *J. Neuroendocrinol.*, **32**, e12821.
39. Passoni, I., Leonzino, M., Gigliucci, V., Chini, B. and Busnelli, M. (2016) Carbetocin is a functional selective Gq agonist that does not promote oxytocin receptor recycling after inducing β-Arrestin-independent internalisation. *J. Neuroendocrinol.*, **28**.
40. Dykens, E.M., Miller, J., Angulo, M., Roof, E., Reidy, M., Hatoum, H.T., Willey, R., Bolton, G. and Korner, P. (2018) Intranasal carbetocin reduces hyperphagia in individuals with Prader-Willi syndrome. *JCI Insight*, **3**, e98333.
41. Andrieu, D., Meziane, H., Marly, F., Angelats, C., Fernandez, P.A. and Muscatelli, F. (2006) Sensory defects in Necdin deficient mice result from a loss of sensory neurons correlated within an increase of developmental programmed cell death. *BMC Dev. Biol.*, **6**, 56.
42. Gong, S., Zheng, C., Doughty, M.L., Losos, K., Didkovsky, N., Schambra, U.B., Nowak, N.J., Joyner, A., Leblanc, G., Hatten, M.E. *et al.* (2003) A gene expression atlas of the central nervous system based on bacterial artificial chromosomes. *Nature*, **425**, 917–925.
43. Elands, J., Barberis, C., Jard, S., Tribollet, E., Dreifuss, J.J., Bankowski, K., Manning, M. and Sawyer, W.H. (1988) 125I-labelled d(CH2)5[Tyr(Me)2,Thr4,Tyr-NH2(9)]OVT: a selective oxytocin receptor ligand. *Eur. J. Pharmacol.*, **147**, 197–207.
44. Elands, J., Beetsma, A., Barberis, C. and de Kloet, E.R. (1988) Topography of the oxytocin receptor system in rat brain: an autoradiographical study with a selective radioiodinated oxytocin antagonist. *J. Chem. Neuroanat.*, **1**, 293–302.
45. Miller, J.A. and Zahniser, N.R. (1987) The use of 14C-labeled tissue paste standards for the calibration of 125I-labeled ligands in quantitative autoradiography. *Neuroscience letters*, **81**, 345–350.
46. Thevenaz, P., Ruttimann, U.E. and Unser, M. (1998) A pyramid approach to subpixel registration based on intensity. *IEEE Trans. Image Process.*, **7**, 27–41.